**Journal Article**

**Application of Machine Learning-Assisted Global Optimization for Improvement in Design and Performance of Open Resonant Cavity Antenna**

Dutta, K., Akinsolu, M. O. Akinsolu, Mishra, P. K., Liu, B. and Guha, D.



**Recommended citation:**

Dutta, K., Akinsolu, M. O. Akinsolu, Mishra, P. K., Liu, B. and Guha, D. (2024), 'Application of Machine Learning-Assisted Global Optimization for Improvement in Design and Performance of Open Resonant Cavity Antenna', IEEE Open Journal of Antennas and Propagation, vol. 5, no. 3, pp. 693-704. doi: 10.1109/OJAP.2024.3385675.

Received 31 December 2023; revised 25 March 2024; accepted 31 March 2024. Date of publication 4 April 2024; date of current version 27 May 2024.

*Digital Object Identifier 10.1109/OJAP.2024.3385675*

# Application of Machine Learning-Assisted Global Optimization for Improvement in Design and Performance of Open Resonant Cavity Antenna

**KOUSHIK DUTTA [1] (Senior Member, IEEE), MOBAYODE O. AKINSOLU [2] (Senior Member, IEEE), PUNEET KUMAR MISHRA [3] (Senior Member, IEEE), BO LIU [4] (Senior Member, IEEE), AND DEBATOSH GUHA [5,6] (Fellow, IEEE)**

[1] Electronics and Communication Engineering Department, Netaji Subhash Engineering College, Kolkata 700152, India

[2] Faculty of Arts, Computing and Engineering, Wrexham University, LL11 2AW Wrexham, U.K.

[3] Systems Integration Group, U. R. Rao Satellite Centre, Bengaluru 560017, India

[4] James Watt School of Engineering, University of Glasgow, G12 8QQ Glasgow, U.K.

[5] Institute of Radio Physics and Electronics, University of Calcutta, Kolkata 700009, India

[6] Department of Electronics and Communication Engineering, National Institute of Technology Jaipur, Jaipur 302017, India

CORRESPONDING AUTHOR: K. DUTTA (e-mail: koushikdutt@ieee.org)

This work was supported in part by the Scheme of Abdul Kalam Technology Innovation National Fellow of INAE/DST-SERB, Government of India, and in part by DST-SERB Project, Government of India.

**ABSTRACT** Open resonant cavity antenna (ORCA) and its recent advances promise attractive features and possible applications, although the designs reported so far are solely based on the classical electromagnetic (EM) theory and general perception of EM circuits. This work explores machine learning (ML)-assisted antenna design techniques aiming to improve and optimize its major radiation parameters over the maximum achievable operating bandwidth. A state-of-the-art method, e.g., parallel surrogate model-assisted hybrid differential evolution for antenna synthesis (PSADEA) has been exercised upon a reference ORCA geometry revealing a fascinating outcome. This modifies the shape of the cavity which was not predicted by EM-based analysis as well as promising significant improvement in its radiation properties. The PSADEA-generated design has been experimentally verified indicating 3dB-11dB improvement in sidelobe level along with high broadside gain maintained above 17 dBi over the 18.5% impedance bandwidth of the ORCA. The new design has been theoretically interpreted by the theory of geometrical optics (GO). This investigation demonstrates the potential and possibilities of employing artificial intelligence (AI)-based techniques in antenna design where multiple parameters need to be adjusted simultaneously for the best possible performances.

**INDEX TERMS** Artificial intelligence, machine learning, high gain antenna, optimization technique, resonant cavity antenna

## I. INTRODUCTION

OPEN resonant cavity antenna (ORCA) is a class of high-gain antenna which is becoming increasingly popular due to its attractive features and small footprint. It consists of a resonant cavity formed between a ground plane and a superstrate where a microstrip patch, dielectric resonator, radiating slot, or open-ended waveguide could be used as a primary radiator [1], [2], [3], [4], [5], [6], [7], [8], [9], [10], [11], [12], [13], [14], [15], [16], [17], [18], [19], [20], [21], [22], [23], [24], [25], [26], [27], [28], [29], [30], [31], [32]. The high gain property is achieved through multiple reflections like in a Fabry-Perot cavity [12], [13], [14], [15], [16], [17], [18], [19], [20], [21], [22]. Instead of a partially reflective surface [1], [2], [3], [4], [5], [6], [7], [8], [9], [10], [11], [12], [13], [14], [15], [16], [17], [18], [19], [20], [21], [22], [23], [24], [25], [26], [27], a nontransparent superstrate was also tested successfully [28], [29], [30], [31], [32].

A recent study introduced an additional vertically erected wall and reported high gain consistently over a large bandwidth [32]. That work [32] employed geometrical optics (GO) to optimize the field confinement within the cavity and electromagnetic (EM) analysis of cavity modes. That resulted in a specific cavity shape along with that of the superstrate structure and enlightened us about the ability enormous potential of the new ORCA geometry. However, it demands high-quality optimization of multiple parameters simultaneously to obtain the best possible performance over a wide range of frequencies. This work actually targets optimizing each design parameter and achieving the best possible or near to the best possible antenna structure. Following the present trend in science and engineering, we have explored machine learning (ML), or artificial intelligence (AI) assisted techniques more effectively.

AI-based antenna design is becoming more prevalent [33], [34] as it provides faster optimization speed and better quality solutions compared to the conventionally available methods [33], [34]. Nowadays, the most widely used AI-based antenna optimization methods combine evolutionary computation and supervised learning in a single framework to maximize the pros of both techniques [34], [35], [36], [37]. Usually, the computation part of the framework is an evolutionary algorithm like differential evolution (DE) or particle swarm optimization (PSO), which explores the antenna design space. The supervised learning part is a regression technique like Gaussian process regression (or Kriging), support vector regression (SVR), and radial basis function networks (RBFN) [34], [35], [36], [37]. For the antenna optimization framework, the researchers prefer methods such as PSO-SVR, DE-RBFN [38], deep learning implemented with multilayer neural networks [34], and domain knowledge-guided search [39], [40].

The present design employs the third generation of the 'surrogate model-assisted hybrid differential evolution for antenna synthesis' (SADEA) algorithm [41]. This is now in its fifth installment and is called 'parallel SADEA' or simply PSADEA [42], [43]. Its core elements are Gaussian Process (GP)-based supervised learning and evolutionary computation anchored by DE. The reason for selecting PSADEA in this work stems from its ability to successfully address a few practical antennas (even when a designer has little or no knowledge of the feasibility or realizability)such as base station antennas [44], dual-polarized folded antennas [45], reconfigurable antennas [46], substrate integrated waveguide antennas [47], and metasurface-based antennas [48]. In addition, the computational cost of PSADEA is attractive compared to [49], [50], [51], for example being 8 times faster than DE and PSO [43], [52]. Unlike DE and PSO, PSADEA is competently applicable to complex antenna structures [47], [53]. It may be relevant to mention that the improved efficiency of PSADEA originates from 'surrogate model-aware evolutionary search' (SMAS) framework (to

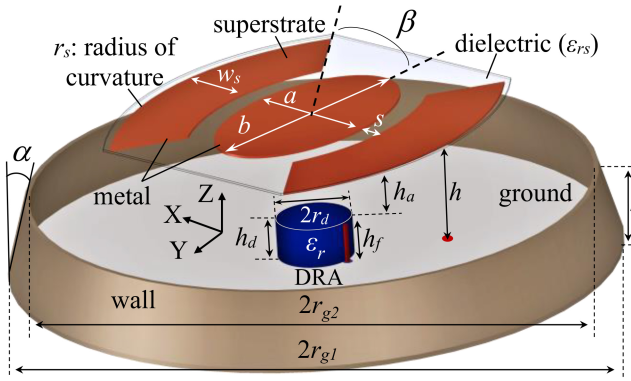


**FIGURE 1.** Isometric 3D view of the OCRA under PSADEA optimization. Parameters: $r_{g1}$=116, $r_{g2}$=108, $h_a$=37, $h_d$=$r_d$=10, $h_w$=34, $h_f$ =10, $h = h_f + h_d$, a = 46, $b$ = 92,$r_s$= 45, $w_s$ = 22, $s$ = 10, $\beta$ = 25°, $\varepsilon_r$ = 10, $\varepsilon_{rs}$ = 2.55. (all dimensions are in mm).

**TABLE 1.** Search ranges of the design parameters and the optimal design by PSADEA (All sizes in mm except where stated otherwise).

| Parameters # | Initial value * | Range of variation | | PSADEA-Optimum |
|---|---|---|---|---|
| | | Lower Bound | Upper Bound | |
| $r_{g1}$ | 116 | 100 | 140 | **101.65** |
| $r_{g2}$ | 108 | 90 | 150 | **115.84** |
| $h_w$ | 34 | 10 | 60 | **40.63** |
| $h_a$ | 37 | 30 | 45 | **36.69** |
| $a$ | 46 | 40 | 55 | **46.44** |
| $r_e$=$b$/$a$ | 2 units | 1 unit | 3 units | **1.7 units** |
| $w_s$ | 22 | 10 | 30 | **28.95** |
| $s$ | 10 | 5 | 20 | **13.4** |
| $\beta$ | 25 deg | 20 deg | 50 deg | **33.16deg** |
| $r_s$ | 45 | 40 | 50 | **49.82** |

have an optimal co-working of the global search driven by DE), and the surrogate modeling (carried out by GP) [54], and self-adaptive use of three complementary DE mutation operators (to have a better balance between the exploration and exploitation of the antenna design space) [42], [43].

The result of the ML-based investigation provides an improved structure with a completely new feature compared to the reference antenna [32]. The novelty of the present work lies in restructuring the cavity geometry and also in achieving significantly improved radiation properties, especially in terms of its side lobe level (SLL). These characteristics have been verified with the help of the traditional GO method and also through a series of experiments. The results indicate a fractional impedance bandwidth of 18.5% (3.55 GHz to 4.3 GHz), minimum in-band broadside gain of 17.4 dBi, and maximum in-band SLLof −17 dB. The improvement may be understood if compared with the reference ORCA showing fractional impedance bandwidth of 15.46% (3.61 GHz to 4.22 GHz), a minimum in-band broadside gain of 15.56 dBi,and a maximum in-band SLL of-8.18 dB.

## II. BACKGROUND AND OBJECTIVE OF THIS STUDY

This study aims to apply an optimization algorithm to our previously reported ORCA shown in Fig. 1 [32]. This embodies a probe-fed cylindrical dielectric resonator antenna (DRA) as a primary radiator loaded by a shaped superstrate, and a conical cavity wall. This multiparametric design and its interdependencies appear too sensitive to the sweeping of some of the values listed in Table 1. This table furnishes a set of parameters obtained in [32] by sensitivity analysis. We found that these design parameters highly affect the antenna performance and verified experimentally. But such an experience-driven trial or tuning of parameters leading to the best possible design appears to be impractical.

An ML-driven technique, we, therefore, believe would help in reaching a relatively improved and optimized design of this reference antenna geometry (Fig. 1) and address the challenges in terms of its physical topology and electromagnetic characterization. These challenges include but are not limited to (i) unclear interdependencies and electromagnetic interactions between the ORCA's design parameters that cannot be feasibly ascertained via design experience and parameter sweeps, (ii) maintaining a large FBW with high broadside gain and very low SLL for a similar topology to the reference ORCA design, and (iii), maintain a similar or lower profile to the reference ORCA design.

For the present exploration, a set of design parameters and their search ranges have been chosen and shown in Table 1. The goal is to optimize the same in order to maximize the fractional impedance bandwidth (FBW) over the frequency range of 3.5 GHz to 4.3 GHz, with $\leq -10$ dB in-band return loss, subject to a minimum in-band broadside gain ($G_{broad}$) of 16 dBi or higher, and a maximum allowable in-band SLL of $-14$ dB or lower.

## III. DESIGN OBTAINED USING MACHINE LEARNING-ASSISTED GLOBAL OPTIMIZATION

Several numerical methods that can be employed for local or global optimization of antennas are available in the literature [52]. Typically, in a simulation-driven optimization used for electromagnetic structure, an adequate initial design geometry identified a priori is required as an anchor or starting point for local optimizers. AI plays an important role in the present perspective of advanced machine learning-assisted global optimization procedures.

### A. BACKGROUND OF OPTIMIZATION: TECHNIQUES AND STUDIES

In contrast to local optimization methods, global optimization methods for antennas do not involve any initial or starting configuration. However, they usually demand a large, sometimes unaffordable, number of full-wave EM simulations [55]. For the proposed ORCA structure, it costs about 20 minutes on average to complete a full-wave EM simulation and a typical run using a global optimization may last for 8 to 12 weeks without any guarantee of useful outcomes. Hence, conventional local and *global* optimization methods are not the right fit for the targeted goal.

In the last decade or so, AI techniques, specifically, machine learning (ML) have been introduced extensively into the optimization frameworks of standard global numerical optimization methods for antenna design, especially evolutionary algorithms (EAs). They were reported to reduce the overall computational cost [35], [36], [37], [39]. The most popular approach is surrogate model-based optimization. The surrogate models are also referred to as metamodels and are constructed using ML techniques. They are computationally cheap and can approximate the antenna behavior replacing the expensive feature of optimization in the commercial full-wave simulators. Nowadays, several ML-assisted antenna optimization methods are available [39], [56], [57], [59], [59], [60]. However, many of them are not very generic, are reliant on many ad-hoc processes, or have limitations on the number of design variables, or the range for surrogate modeling and search. Therefore, a more generic AI-based method 'PSADEA' has been employed whose main elements and workflow are elaborately discussed in [42], [43]. In the PSADEA-driven optimization of the proposed ORCA, the goal is the minimization of the fitness function $F_{ORCA}$, taking the specifications for $G_{broad}$, $SLL$, and $FBW$ into account.

### B. PSADEA-DRIVEN DESIGN OF THE PROPOSED ORCA

A GP-based surrogate model in PSADEA works as follows [42], [43]: given a set of antenna design geometry ($x = [x_1, \ldots, x_n]$) and EM simulation results ($y = [y_1, \ldots, y_n]$), to predict the performances ($y = f(x)$) for a candidate design $x$, $y(x)$ is modeled as a Gaussian distributed stochastic variable with a mean of $\mu$ and a variance of $\sigma^2$. If $y(x)$ is continuous, the function values ($y(x_p)$ and $y(x_q)$) of any two candidate designs such as $x_p$ and $x_q$ can be expected to be close if they have a high correlation. To derive the correlation, a Gaussian correlation is used as follows:

$$Corr(x_p, x_q) = e^{-\sum_{t=1}^{d} r_t \left|x_p^t - x_q^t\right|^{\xi_t}}$$
$$\text{for } r_t > 0,\ 1 \leq \xi_t \leq 2 \tag{1}$$

where the dimension of $x$ is $d$ and $r_t$ (correlation parameter) evaluates how quickly the decorrelation occurs as $x_a$ moves in the $t$ direction. $\xi_t$ relative to $x^t$ accounts for the smoothness of the function. Maximization of the likelihood function that $y = y^i$ at $x = x^i (i = 1, \ldots, n)$ is used to derive $r_t$ and $t$. Hence, for a candidate design ($x^{**}$), the prediction of the performance ($y(x^{**})$) is:

$$\widehat{y}(x^{**}) = \widehat{\mu} + m^T M^{-1}(y - Z\widehat{\mu}) \tag{2}$$

where

$$M_{p,q} = Corr(x_p, x_q), p, q = 1, 2, \ldots, n \tag{3}$$
$$h = \left[Corr(x^{**}, x_1), Corr(x^{**}, x_2), \ldots, Corr(x^{**}, x_n)\right] \tag{4}$$
$$\widehat{\mu} = \left(Z^T M^{-1} Z\right)^{-1}\left(Z^T M^{-1} y\right) \tag{5}$$

The mean squared error associated with the prediction uncertainty is:

$$MSE = \widehat{\sigma}^2\left[Z - m^T M^{-1} m + \left(Z - m^T M^{-1} m\right)^2 \left(Z^T M^{-1} Z\right)^{-1}\right] \tag{6}$$

where

$$\widehat{\sigma}^2 = (y - Z\widehat{\mu})^T M^{-1}(y - Z\widehat{\mu}) n^{-1} \tag{7}$$

GP modeling has a computational complexity of $\mathcal{O}(n_{iteration}, K^3, d)$, where $n_{iteration}$ and $K$ are the number of iterations completed in the optimization of the hyperparameter and the available training data points, respectively [61].

Several prescreening methods are available for assessing the quality of a candidate design for the predicted value in (2) and the prediction uncertainty in (6) [61]. The lower confidence bound (LCB) method [62], is used in PSADEA. Such that if the predictive distribution of $y(x)$ is $N(\widehat{y}(x), MSE)$ then the LCB prescreening of $y(x)$ is:

$$\widehat{y}(x) - \omega\sqrt{MSE} \tag{8}$$

where $\omega$ is a constant that is usually set to two to balance exploitation and exploration [61].

The DE-based search in PSADEA works as follows [63]: given that $P_{ORCA}$ is the design population for the ORCA optimization such $x \in \mathbb{R}^d$ is a set of parametric values for a candidate ORCA design, to produce, $C$, a child solution for $x$, mutation first occurs using three complementary DE mutation operators (DE/best/1, DE/current-to-best/1, and DE/rand/2, in (9), (10) and (11), respectively [63]) self-adaptively:

$$v^i = x^{best} + F.\left(x^{r1} - x^{r2}\right) \tag{9}$$

$$v^i = x^i + F.\ \left(x^{best} - x^i\right) + F.\left(x^{r1} - x^{r2}\right) \tag{10}$$

$$v^i = x^{r1} + F.\ \left(x^{r2} - x^{r3}\right) + F.\left(x^{r4} - x^{r5}\right) \tag{11}$$

where $v^i$ is the $i$th mutant vector, $x^{best}$ is the best candidate solution in the current population $P_{ORCA}$, $F \in (0,\ 2]$ is a control parameter, often called the scaling factor, $x^{r1}$, $x^{r2}x^{r3}$, $x^{r4}$, and $x^{r5}$ randomly selected mutually exclusive solutions from $P_{ORCA}$.

Then crossover takes place as follows to generate $C$, the child solution:

1) Randomly select a variable index $j^{rand} \in \{1, \ldots, d\}$,

2) For each $j = 1$ to $d$, generate a uniformly distributed random number $rand$ from $(0,\ 1)$ and set:

$$C_j = \begin{cases} v_j & \text{if } (rand \ \leq\ C_R) |\ j = j_{rand} \\ x_j & \text{otherwise} \end{cases} \tag{12}$$

where $C_R \in [0,\ 1]$ is the crossover rate (a constant).

The PSADEA-driven optimization flow diagram is shown in Fig. 2, and the steps are summarized as follows:

*Step 1:* 50 design solutions are sampled from the ORCA's design space using the Latin hypercube sampling (LHS) method [64]. These designs are then simulated to obtain their performances to create an initial database.

*Step 2:* If a predetermined stopping criterion, e.g., the maximum number of EM simulations is met, PSADEA outputs the best design solution from the database. Otherwise, Step 3 is carried out.

*Step 3:* Select $\tau$ top-ranked design solutions from the database.

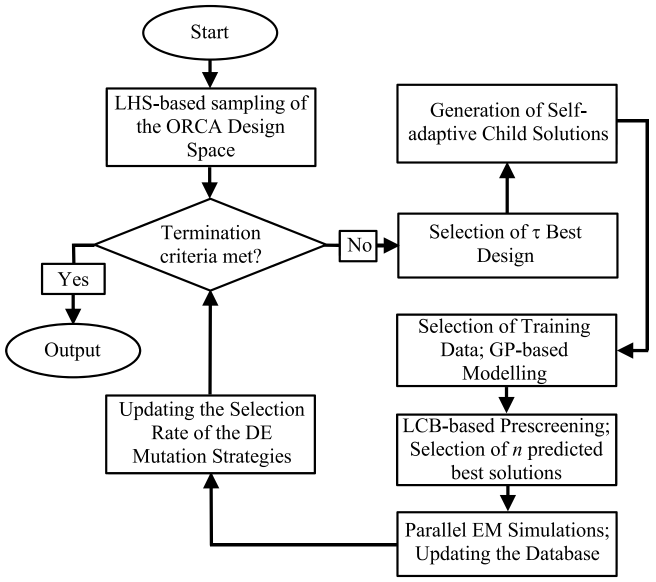


**FIGURE 2.** Flow diagram of PSADEA.

*Step 4:* Generate child solutions by applying the DE mutation operators in (9), (10), and (11), self-adaptively to the design solutions selected in Step 3.

*Step 5:* For every candidate in each of the child populations, from the database, GP-based surrogate models are constructed using the nearest designs (determined using Euclidean distance) and their performance values as the training data.

*Step 6:* To handle prediction uncertainty, the generated child solutions from Step 4 are prescreened using the surrogate models from Step 5 and the LCB method [62]. The three best design solutions are then selected based on the LCB values.

*Step 7:* The selected best solutions are simulated in parallel, and their simulation results are added to the database.

More details about the PSADEA workflow can be found in [42], [43]. PSADEA may be applied to most of the common antenna geometry but with a limitation when the number of design parameters is very high, e.g., >50. The reason behind this is increased training time for GP [61]. The present case of targeted ORCA embodies 10 design parameters, which are comfortably handled by this PSADEA.

In this PSADEA-driven optimization, the goal is the minimization of the fitness function, $F_{ORCA}$, stated as follows:

$$\begin{aligned} F_{ORCA} = -FBW + w\{&\max([14\ dBi - G_{broad}, 0]) \\ &+ \max([SLL + 14\ dB, 0])\} \end{aligned} \tag{13}$$

where $w$ is the penalty coefficient set to 50 to preferentially ensure that the specifications for $G_{broad}$ and $SLL$ are focused on first in the optimization process by penalizing $F_{ORCA}$ heavily if they are violated. Then the optimization run

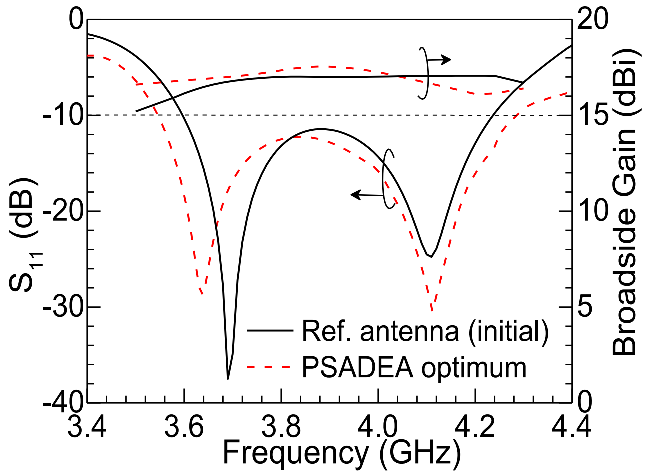


**(a)**

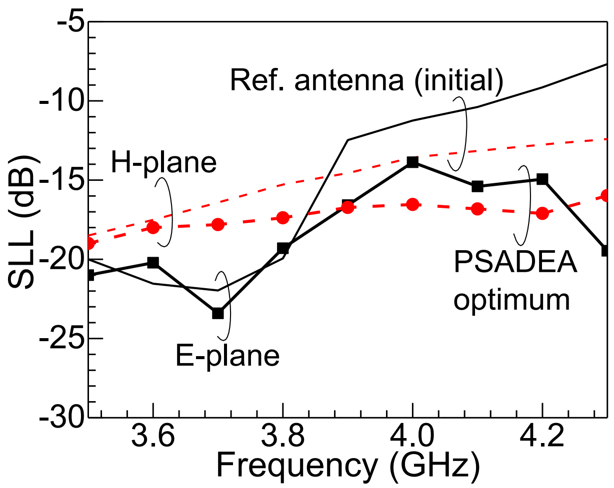


**(b)**

**FIGURE 3. Comparison of the reference antenna with the PSADEA-optimized OCRA over the frequency band for their: (a) $S_{11}$ and boresight gain, (b) E- and H-plane SLL. Parameters as in Table 1.**

focuses on the maximization of *FBW* immediately after the specifications for $G_{broad}$ and *SLL* have been satisfied. All other optimization settings are the default settings in [42] and [43]. The geometry, electromagnetic characterization, and physical implementation of this ML-assisted AI-driven design are discussed below.

### C. OPTIMIZED RESULTS AND NEW CONFIGURATION

For the optimization run, the antenna model was built and discretized in CST-MWS [55] using a total of about 7,250,000 hexahedral cells having a mesh density of 15 mesh cells per wavelength. Each cycle costs about 20 min (from a wall clock) on average on a workstation with an Intel eight-core i9-9900K 3.6 GHz CPU and 32 GB RAM. After 1095 full-wave EM simulations, PSADEA obtained a design that showed a satisfactory performance (meeting both $G_{real}$ and *SLL* specifications and having an *FBW* of 15.6% (3.55 GHz to 4.15 GHz). It then converged after 2771 full-wave EM simulations to produce the design (PSADEA-Optimum) reported in Table 1 having an *FBW* of 19.1% (3.54 GHz to 4.29 GHz), $G_{broad}$ of 17.5 dBi, and *SLL* of −15.62dB. Note

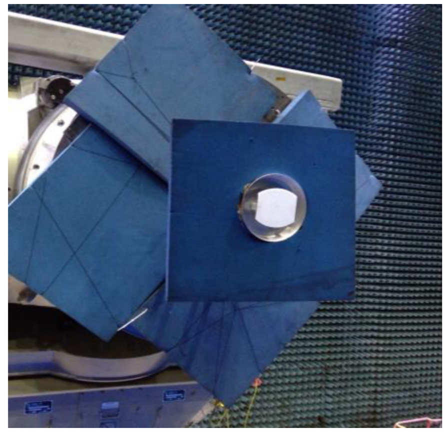

**(a)**

**(b)**

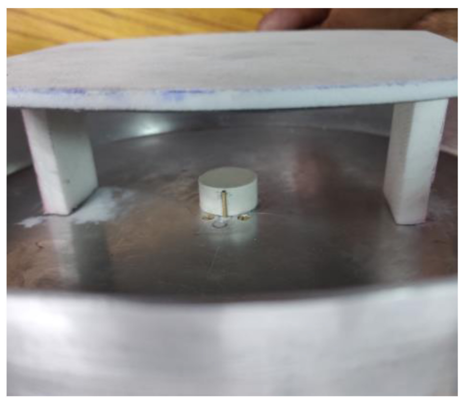

**(c)**

**FIGURE 4. Fabricated antenna prototypes and experimental setup. (a) Setup for radiation pattern measurement, (b) top view of the fabricated antenna prototype, (c) perspective view of the antenna prototype. All parameters are as in PSADEA-optimum values in Table 1.**

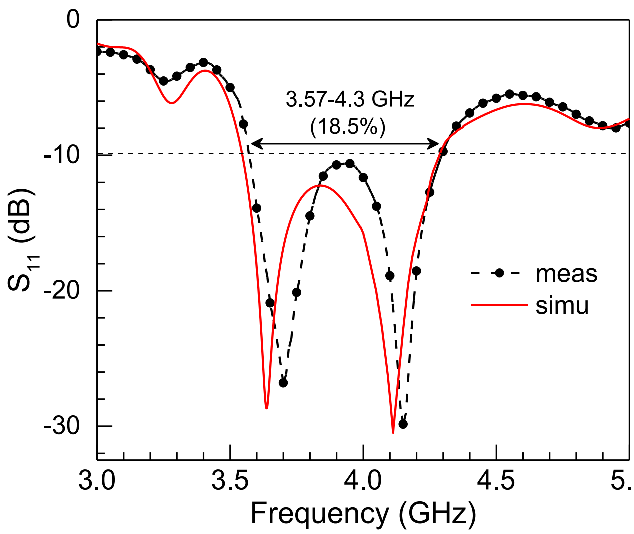


(a)

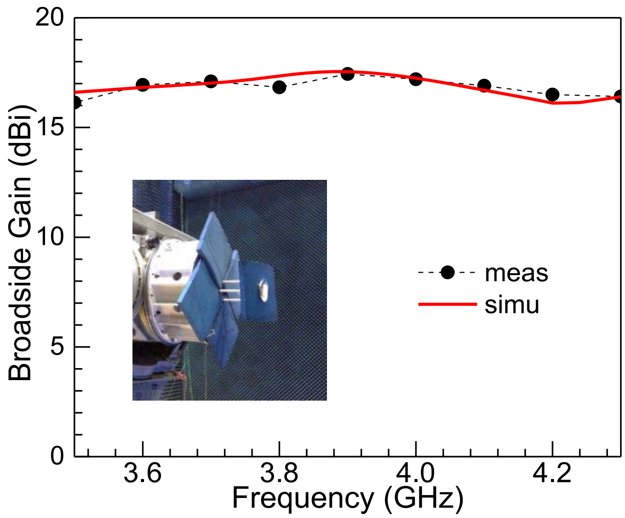


(b)

**FIGURE 5.** Measured $S_{11}$ and gain variation as a function of frequency and compared with the simulated prediction: (a) $S_{11}$, (b) boresight gain. All parameters as in Fig. 1 and Table 1.

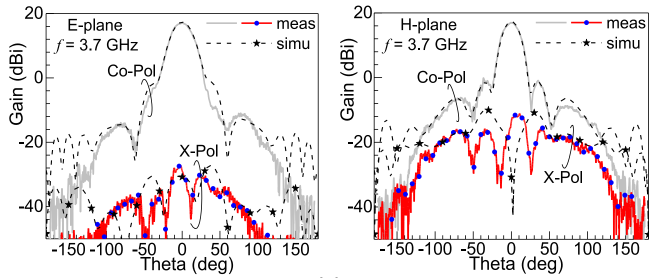


(a)

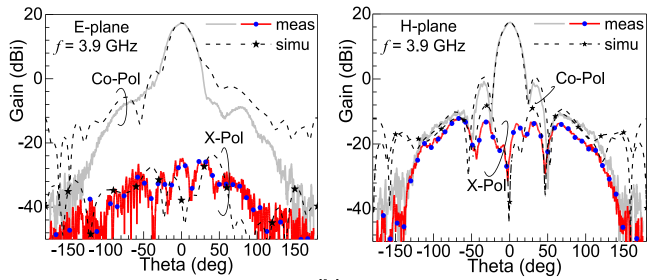


(b)

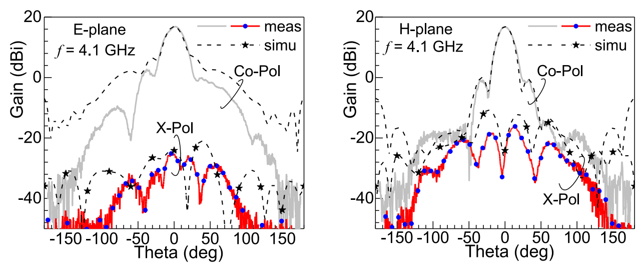


(c)

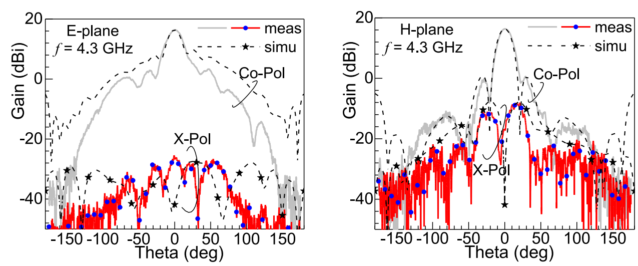


(d)

**FIGURE 6.** E- and H-plane radiation patterns at (a) 3.7 GHz, (b) 3.9 GHz, (c) 4.1 GHz, and (d) 4.3 GHz. Parameters as in Fig. 1 and Table 1.

that PSADEA does not follow a one-shot sampling method. Instead, the samples are obtained self-adaptively using the machine learning technique [42], [43].

Table 1 shows the optimized parameters obtained using PSADEA. This shows some changes in the optimized values compared to the reference antenna, and one parameter appears drastically different from the reference design and that is the configuration of the cavity wall. The PSADEA-optimized geometry proposes a vertical wall to be inclined outward which is in contrast with the reference antenna conceived and analyzed earlier with an opposite inclination of the vertical wall. This results in $rg_2 > rg_1$ with $\alpha \rightarrow -$ve (reference antenna [32]: $rg_2 < rg_1$ with $\alpha \rightarrow +$ve). The impact of the significant change in the PSADEA-based design with respect to the reference configuration has been thoroughly examined in Fig. 3. The $S_{11}$ and gain characteristics compared in Fig. 3(a) appear mutually comparable or with very little variation. But a significant improvement in SLL value is revealed in Fig. 3(b), which is more predominant near the higher frequencies, over both E- and H-planes. The predicted improvement of SLL is about 6dB over the E-plane and 5dB over the H-plane.

## IV. EXPERIMENTS AND RESULTS

A set of prototypes and associated measurement setups are shown in Fig. 4. The metallic cavity structure is made of a thin aluminum sheet and a cylindrical DRA is machined from Emerson Cuming's HiK $\varepsilon_r$=10 material. The superstrate

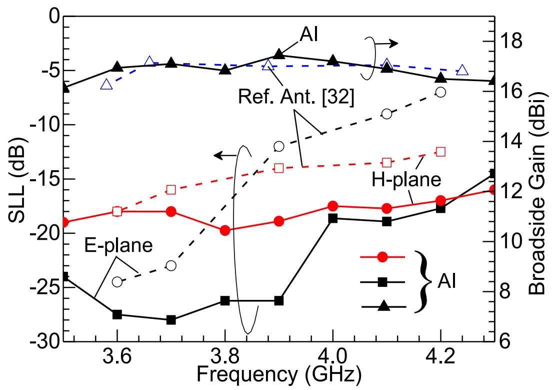


**FIGURE 7.** Measured E- and H-plane SLL values compared with reference antenna. All parameters as in Fig. 1 and Table 1.

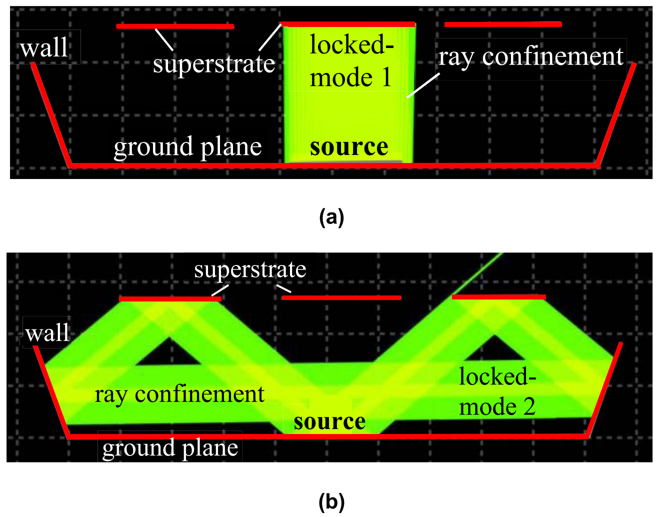


**FIGURE 8.** Demonstration of energy confinement due to the possible locked-modes in OCRA with inclined cavity wall and superstrate due to: (a) conventional Fabry-Perot cavity (locked-mode-1), (b) tilted cavity wall (locked-mode-2). Results are obtained by using GO based simulator [66].

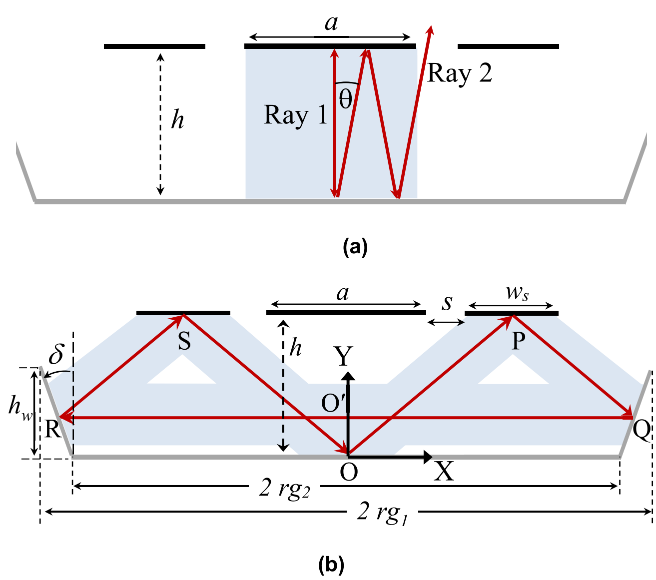


**FIGURE 9.** Schematic representation of the locked-modes due to: (a) conventional Fabry-Perot cavity (locked-mode-1), (b) tilted cavity wall (locked-mode-2).

geometry is etched from a Taconic TLX $\varepsilon_{rs}$=2.55 substrate. It is symmetrically placed with the support of a pair of Rohacell foam spacers (Fig. 4(c)). The measurements are conducted using Agilent's E8363B network analyzer and an automated anechoic chamber.

The measured $S_{11}$ characteristics of the prototype, depicted in Fig. 5(a) ensure the predicted operating band from 3.57 GHz to 4.3 GHz. Fig. 5(b) depicts measured gain over the entire band. The excellent mutual agreement bears the signature of the authenticity of the PSADEA prediction. The detailed radiation characteristics are studied in Fig. 6 at four different frequencies with equal intervals over the entire bandwidth. The experimental set-up and the large fixture holding the antenna under test restricted our measurement beyond 150° of azimuth. Even then, the measured co-polar values around 150° reveal a related mismatch with the simulated curve. However, the overall comparison between measurements and AI-based prediction is quite satisfactory. The measured data finally establish the superiority of the AI-based design as examined in Fig. 7. The aim of the design, as stated above, was to optimize the antenna geometry based on the best possible radiation, i.e., lowest SLL and optimum antenna gain without compromising the operating bandwidth. Fig. 7 ensures no sacrifice in gain with respect to the reference antenna but with a remarkable improvement in SLL. In the E-plane, the relative improvement is prominent on the higher side of the spectrum, varying from 3dB-11dB with the mid-band improvement of 14 dB. The H-plane feature is found to be improved by 5 dB throughout the spectrum, except on the lower edge of the operating band. Typically, 93-95% radiation efficiency has been confirmed near both resonances based on experimental investigations. This followed the method in [65] using the Wheelers Cap technique.

## V. AI-DRIVEN DESIGN INTERPRETED BY GEOMETRICAL OPTICS

The promising improvements in radiation, especially in the SLL characteristics, as discussed in the previous section, are caused by the PSADEA-obtained new ORCA geometry. Here, we have tried to justify the same using classical geometrical optics (GO) based analysis [32]. A robust physical insight, justifying the PSADEA-obtained structure has also been developed.

We understand that the high gain feature of a Fabry-Perot or resonant cavity antenna is caused by multiple reflection and field confinement mechanisms. The same occurring in the PSADEA-obtained structure confinement has been investigated using a GO simulation tool [66]. Fig. 8 reveals the study indicating two locked modes. Mode 1 (Fig. 8(a)) is straightforward like a traditional Fabry-Perot cavity where

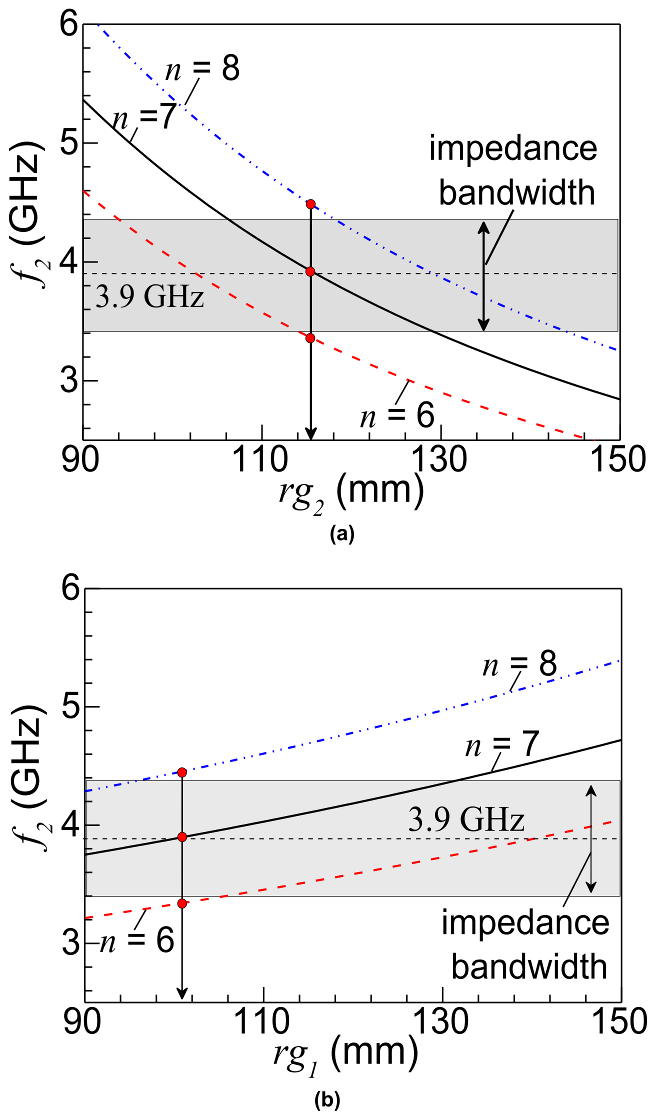


**FIGURE 10.** Theoretical estimation of cavity wall dimensions by using proposed GO based analysis that plots resonance frequency ($f_2$) of locked mode-2 for $n$=6, 7, and 8. (a) $f_2$ vs $r_{g2}$, (b) $f_2$ vs $r_{g1}$. All other parameters are as in PSADEA-optimum values in Table 1.

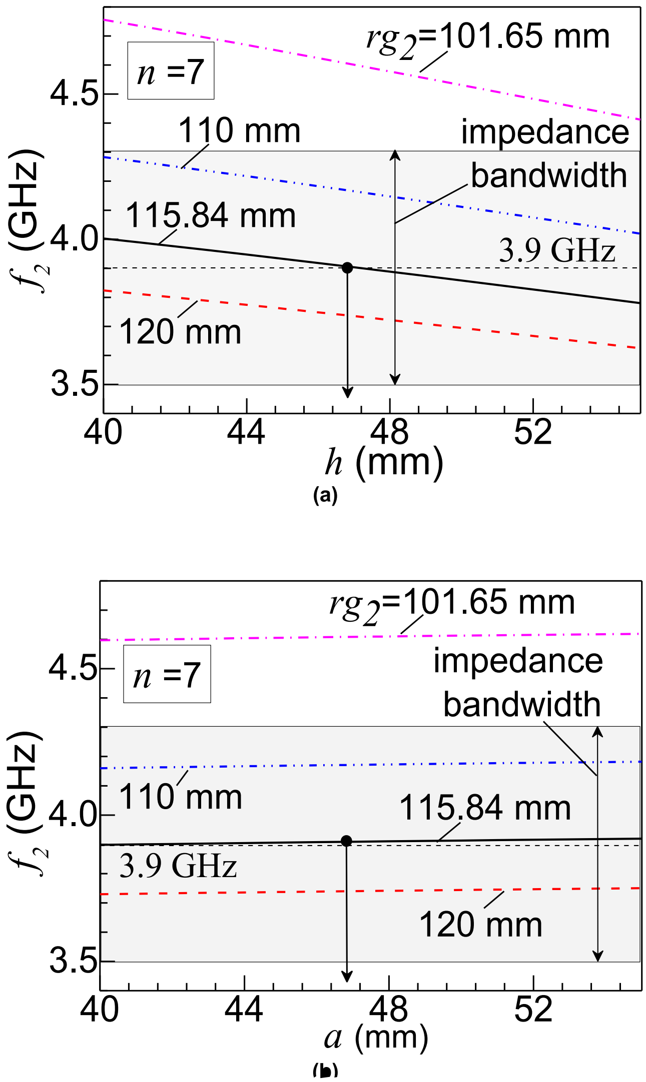


**FIGURE 11.** Theoretical estimation of superstrate height ($h$) and size (a) by using proposed GO based analysis that plots resonance frequency ($f_2$) of locked mode-2 for different antenna parameters at $n$=7: (a) $f_2$ vs $h$ for different $r_{g2}$ values, (b) $f_2$ vs a for different $r_{g2}$ values. All other parameters are as in PSADEA-optimum values in Table 1.

the cavity wall plays no role. Locked mode 2 (Fig. 8(b)) is observed here for the first time and this is caused by the new (AI-driven) shape of the cavity wall. Locked modes-1 and −2 are schematically represented in Figs. 9(a) and (b) respectively. Ray1 with incident angle $\theta \approx 0$ experiences an infinite number of reflections and hence ensures the fullest confinement, represented by the shaded region. Its related resonance condition is straightforward and already discussed in [32]. But mode-2 is completely new to us and its resonance condition reveals some interesting features as discussed below.

The total round-trip phase shift of the rays shown in Fig. 9(b) is

$$\mathrm{OPQRSO}(2\pi/\lambda_2) = 2n\pi \tag{14}$$

with

$$\begin{aligned}\mathrm{OPQRSO} = {} & \sqrt{(a+2s+w_s)^2+(2h)^2}+\sqrt{\left(3rg_2-rg_1\right)^2} \\ & +\sqrt{(2h-h_w)^2+\left(3rg_2-rg_1-a-2s-w_s\right)^2}\end{aligned} \tag{15}$$

The above derivation demands a few steps: OPQRSO=2OPQO′=2(OP+PQ+QO′); with coordinates: O(0,0); P(a/2+$s$+$w_s$/2, $h$); Q($rg_2$+($rg_2$-$rg_1$)/2, $h_w$/2); O′(0, $h_w$/2). Here, Q and R represent the midpoint of the cavity configuration. The parameters obtained by the AI-driven method [42] are shown in Table 1 and they yield

$$f_2 = nc/\mathrm{OPQRSO} \cong 0.56\ n(\text{in GHz}) \tag{16}$$

where $f_2$ is the predicted resonance frequencies as a function of integer $n$, and $c$ is the velocity of light in free space. Based

**TABLE 2.** Present AI-driven design compared with previous conventional structures.

| Ref. | Antenna Size | Operating Band | Superstrate | Primary Radiator | Cavity Wall | design used GO | Use of AI/ML | BW (%) | Gain (dBi) | SLL (dB) | |
|---|---|---|---|---|---|---|---|---|---|---|---|
| | | | | | | | | | | E-plane | H-plane |
| [7] | 2.4λ×2.4λ×0.6λ | X | FSS | Patch | No | × | × | 22.5 | 7–14 | −12 | −10 |
| [67] | 2λ×2λ×0.5λ | V | dielectric | Patch | No | × | × | 6.7 | 8–14.6 | −8 | −12 |
| [68] | 8λ×8λ | Ka | metal grid | waveguide | No | × | × | 10 | 10–16 | −12 | −20 |
| [69] | 8λ×8λ×1.6λ | V | ring PRS | SIW-feed | No | × | × | 17.8 | 17–21 | −10 | −12 |
| [70] | 6λ×6λ×2.2λ | X | dielectric/slab-sheet | Patch | No | × | × | 12.7 | 10–20 | −14 | −22 |
| [30] | 2.5λ×2.5λ×0.5λ | S | printed metal film (engineered) | DRA | No | × | × | 19 | 8–13 | −10 to −5 | −28 to −6 |
| [32] | 2.8λ×2.8λ×0.5λ | S | printed metal film (engineered) | DRA | Yes, flared inward | √ | × | 18 | 16.9–17.2 | −25 to −7 | −18 to −3 |
| **Present** | 2.8λ×2.8λ×0.5λ | S | printed metal film (engineered) | DRA | Yes, flared **outward** | **√** | **√** | **18.5** | **16.9-17.4** | **-28 to -18** | **-20 to -17** |

on Table 1, the possible $f_2$ values are 3.36GHz, 3.92GHz, and 4.48GHz with $n = 6$, 7, and 8, respectively, which fall within the range of our design frequencies.

An interesting study has been executed in Figs. 10 and 11 which portrays the theoretical variation of $f_2$ as a function of some sensitive dimensions. In Fig. 10(a), the targeted operating frequency band is marked as a shaded region. The optimum $rg_2$ that predicts a maximum coverage (with $n$=6, 7, 8) appears to be 115.5 mm and this value exactly matches with the AI-based prediction $rg_2 = 115.84$mm. A similar examination has been executed in Fig. 10(b) for $rg_1$ and the theoretical prediction of optimum $rg_1$=101mm closely corroborates AI-based value $rg_1$=101.65mm. The studies in Figs. 11(a) and (b) are equally interesting. They theoretically find out the best possible $h$ and a values corresponding to the mid-band frequency which show excellent agreement with PSADEA obtained values (Table 1). The GO-based analysis and the theoretical predictions completely justify the PSADEA algorithm obtained data and give more light on the actual physical insight behind that. It would be relevant to note that, in many cases, scientists failed to physically justify the AI-predicted data. But in our case, a physical insight has been successfully demonstrated.

## VI. CONCLUSION

This study provides us with two-fold benefits. One is the earning of confidence in applying AI-assisted optimization in designing a complex antenna bearing multiple dimensions and geometrical variations. The second one is more important which provides a significant improvement in realizing an open resonant cavity antenna geometry. The reported result may be claimed as the best or nearly the best possible one. Comparison Table 2 endorses the claim. The previous reports embody traditional analysis/simulation-based designs. The present effort employing ML helps in noticeably improving the radiation properties as evident from the four rightmost columns.

## ACKNOWLEDGMENT

Debatosh Guha would like to thank the Indian National Academy of Engineering (INAE)/Department of Science and Technology (DST), Government of India for awarding the Abdul Kalum Technology Innovation National Fellowship and associated research grant for antenna developments. The authors are thankful to the review board for the useful comments and suggestions.

## REFERENCES

[1] G. Von Trentini, "Partially reflecting sheet arrays," *IRE Trans. Antennas Propag.,* vol. 4, no. 4, pp. 666–671, Oct. 1956.
[2] A. P. Feresidis and J. C. Vardaxoglou, "High gain planar antenna using optimised partially reflective surfaces," *IEE Proc. Microw., Antennas Propag.*, vol. 148, no. 6, pp. 345–350, Dec. 2001.
[3] D. Jackson and N. Alexopoulos, "Gain enhancement methods for printed circuit antennas," *IEEE Trans. Antennas Propag.*, vol. 33, no. 9, pp. 976–987, Sep. 1985.
[4] Y. J. Lee, J. Yeo, R. Mittra, and W. S. Park, "Application of electromagnetic bandgap (EBG) superstrates with controllable defects for a class of patch antennas as spatial angular filters," *IEEE Trans. Antennas Propag.*, vol. 53, no. 1, pp. 224–235, Jan. 2005.
[5] Y. Ge, K. P. Esselle, and T. S. Bird, "The use of simple thin partially reflective surfaces with positive reflection phase gradients to design wideband, low-profile EBG resonator antennas," *IEEE Trans. Antennas Propag.*, vol. 60, no. 2, pp. 743–750, Feb. 2012.
[6] A. Foroozesh and L. Shafai, "On the characteristics of the highly directive resonant cavity antenna having metal strip grating superstrate," *IEEE Trans. AntennasPropag.*, vol. 60, no. 1, pp. 78–91, Jan. 2012.
[7] A. Pirhadi, H. Bahrami, and J. Nasri, "Wideband high directive aperture coupled microstrip antenna design by using a FSS superstrate layer," *IEEE Trans. Antennas Propag.,* vol.60, no.4, pp. 2101–2106, Apr. 2012.
[8] R. M. Hashmi, B. A. Zeb, and K. P. Esselle, "Wideband high-gain EBG resonator antennas with small footprints and all-dielectric superstructures," *IEEE Trans. Antennas Propag.*, vol. 62, no. 6, pp. 2970–2977, Jun. 2014.
[9] A. A. BabaR. M. Hashmi, K. P. Esselle, J. G. Marin, and J. Hesselbarth "Broadband partially reflecting superstrate-based antenna for 60 GHz applications," *IEEE Trans. Antennas Propag.*, vol. 67, no. 7, pp. 4854–4859, Jul. 2019.
[10] M. W. Niaz, Y. Yin, S. Zheng, L. Zhao, and J. Chen, "Design and analysis of an ultraminiaturized FSS using 2.5-D convoluted square spirals," *IEEE Trans. Antennas Propag.*, vol. 68, no. 4, pp. 2919–2925, Apr. 2020.

[11] K. S. Chandrashekar, K. Dutta, H. Gajera, S. Poornima, and S. Chandramma, "An analytical approach of designing compact microstrip patch antenna using metal-ring superstrate for wideband and broadside radiations," *AEU-Int. J. Electron. Comm.*, vol. 127, Dec. 2020, Art. No.153437

[12] N. Guérin, S. Enoch, G. Tayeb, P. Sabouroux, P. Vincent, and H. Legay, "A metallic Fabry–Perot directive antenna," *IEEE Trans. Antennas Propag.*, vol. 54, no. 1, pp. 220–224, Jan. 2006.

[13] Y. Sun, Z. N. Chen, Y. Zhang, H. Chen, and T. S. P. See, "Subwavelength substrate-integrated Fabry-Pérot cavity antennas using artificial magnetic conductor," *IEEE Trans. Antennas Propag.*, vol. 60, no. 1, pp. 30–35, Jan. 2012.

[14] K. Konstantinidis, A. P. Feresidis, and P. S. Hall, "Multilayer partially reflective surfaces for broadband Fabry–Perot cavity antennas," *IEEE Trans. AntennasPropag.*, vol. 62, no. 7, pp. 3474–3481, Jul. 2014.

[15] M. L. Abdelghani, H. Attia, and T. A. Denidni, "Dual- and wideband together with Fabry–P'erot resonator antenna for WLAN applications," *IEEE Antennas Wireless Propag. Lett.*, vol. 16, pp. 473–476, 2017.

[16] Z. Liu, W. Zhang, D. Fu, Y. Gu, and Z. Ge, "Broadband Fabry–Perot resonator printed antennas using FSS superstrate with dissimilar size," *Microw. Opt. Technol. Let.*, vol. 50, no. 6, pp. 1623–1627, 2008.

[17] N. Nguyen-Trong, H. H. Tran, T. K. Nguyen, and A. M. Abbosh, "Wideband Fabry–Perot antennas employing multilayer of closely spaced thin dielectric slabs," *IEEE Antennas Wireless Propag. Lett.*, vol. 17, pp. 1354–1358, 2018.

[18] H. Attia, M. L. Abdelghani, and T. A. Denidni, "Wideband and high gain millimeter-wave antenna based on FSS Fabry–Perot cavity," *IEEE Trans. Antennas Propag.*, vol. 65, no. 10, pp. 5589–5594, Oct. 2017.

[19] K. Kanjanasit and C. Wang, "A wideband resonant cavity antenna assembled using a micromachined CPW-fed patch source and a two layer metamaterialsuperstrate," *IEEE Trans. Comp., Pack., Man. Tech.*, vol. 9, no. 6, pp. 1142–1150, Jun. 2019.

[20] K. Dutta and D. Guha, "Fabry–Perot resonant cavity antenna: new theory and design opportunity," in *Proc. URSI Asia-Pacific Radio Sc. Conf.*, 2019, p. 1.

[21] J. G. Marin, A. A. Baba, D. L. Cuenca, J. Hesselbarth, R. M. Hashmi, and K. P. Esselle, "High-gain low-profile chip-fed resonant cavity antennas for millimeter-wave bands," *IEEE Antennas Wireless Propag. Lett.*, vol. 18, no. 11, pp. 2394–2398, Nov. 2019.

[22] L. Zhou, X. Duan, Z. Luo, Y. Zhou, and X. Chen, "High directivityFabry–Perot antenna with a nonuniform partially reflective surface and a phase correcting structure,"*IEEE Trans. Antennas Propag.*, vol. 68, no. 11, pp. 7601–7606, Nov. 2020.

[23] F. Wu and K. M. Luk, "Wideband high-gain open resonator antenna using a spherically modified, second-order cavity," *IEEE Trans. AntennasPropag.*, vol. 65, no. 4, pp. 2112–2116, Apr. 2017.

[24] A. Chatterjee, K. Dutta, S. Chakrabarti, and R. Mittra, "Advanced design of high-gain Fabry–Perot cavity antenna offering wide common impedance and gain bandwidth," *IEEE Antennas Wireless Propag. Lett.*, vol. 22, no. 5, pp. 1214–1218, May 2023,.

[25] A. Lalbakhsh, M. U. Afzal, K. P. Esselle, S. L. Smith, and B. A. Zeb, "Single-dielectric wideband partially reflecting surface with variable reflection components for realization of a compact high-gain resonant cavity antenna," *IEEE Trans. Antennas Propag.*, vol. 67, no. 3, pp. 1916–1921, Mar. 2019.

[26] L. Zhou, X. Duan, Z. Luo, Y. Zhou, and X. Chen "High directivity Fabry–Perot antenna with a nonuniform partially reflective surface and a phase correcting structure," *IEEE Trans. Antennas Propag.*, vol. 68, no. 11, pp. 7601–7606, Nov. 2020.

[27] A. Lalbakhsh, M. U. Afzal, K. P. Esselle, and S. L. Smith, "Low-cost nonuniform metallic lattice for rectifying aperture near-field of electromagnetic bandgap resonator antennas," *IEEE Trans. Antennas Propag.*, vol. 68, no. 5, pp. 3328–3335, May 2020.

[28] K. Dutta, D. Guha, C. Kumar, and Y. M. M. Antar, "New approach in designing resonance cavity high gain antenna using nontransparent conducting sheet as the superstrate," *IEEE Trans. Antennas Propag.*, vol. 63, no. 6, pp. 2807–2813, Jun. 2015.

[29] K. Dutta, D. Guha, and C. Kumar, "Synthesizing aperture fields over engineered metal film superstrate in a resonance cavity antenna for modifying its radiation properties," *IEEE AntennasWireless Propag. Lett.*, vol. 15, pp. 1677–1680, 2016.

[30] K. Dutta, D. Guha, and C. Kumar, "Theory of controlled aperture field for advanced superstrate design of a resonance cavity antenna with improved radiations properties," *IEEE Trans. Antennas Propag.*, vol. 65, no. 3, pp. 1399–1403, Mar. 2017.

[31] K. Dutta, S. Manna, A. Pal, P. K. Mishra, and D. Guha, "Wideband design of a Fabry-Perot cavity antenna with improved features," in *Proc. IEEE Indian Conf.* Antennas*Propag. (InCAP)*, 2018, pp. 1–2.

[32] K. Dutta, P. K. Mishra, S. Manna, A. Pal, and D. Guha, "Geometrical optics-based advanced design of an open cavity resonant antenna,"*IEEE Antennas Wireless Propag. Lett.*, vol. 20, no. 3, pp. 322–326, Mar. 2021.

[33] S. D. Campbell and D. H. Werner, *Advances in Electromagnetics Empowered by Artificial Intelligence and Deep Learning*. Hoboken, NJ, USA: Wiley, 2023.

[34] N. Sarker, P. Podder, M. R. H. Mondal, S. S. Shafin, and J. Kamruzzaman''Applications of machine learning and deep learning in antenna design, optimization, and selection: A review," *IEEE Access*, vol. 11, pp. 103890–103915, 2023.

[35] Q. Wu Y. Cao, H. Wang, and W. Hong, "Machine-learning-assisted optimization and its application to antenna designs: Opportunities and challenges," *China Commun.*, vol. 17, no. 4, pp. 152–164, Apr. 2020.

[36] H. M. El Misilmani, T. Naous, and S. K. Al Khatib, "A review on the design and optimization of antennas using machine learning algorithms and techniques," *Int. J. RF Micro. Comput.-Aided Eng.*, vol. 30, no. 10, Jul. 2020, Art. no. e22356.

[37] M. O. AkinsoluK. K. Mistry, B. Liu, P. I. Lazaridis, and P. Excell, "Machine learning-assisted antenna design optimization: A review and the state-of-the-art," in *Proc. Euro. Conf. Antennas Prop. (EuCAP)*, Copenhagen, Denmark, 2020, pp. 1–5.

[38] A. Massa and M. Salucci, "On the design of complex EM devices and systems through the system-by-design paradigm: A framework for dealing with the computational complexity," *IEEE Trans. Antennas Propag.*, vol. 70, no. 2, pp. 1328–1343, Feb. 2022.

[39] Q. Wu, W. Chen, C. Yu, H. Wang, and W. Hong, "Multilayer machine learning-assisted optimization-based robust design and its applications to antennas and array," *IEEE Trans. Antennas Propag.*, vol. 69, no. 9, pp. 6052–6057, Sep. 2021.

[40] Q. Wu, W. Chen, C. Yu, H. Wang, and W. Hong, "Knowledge-guided active-base-element modeling in machine-learning-assisted antenna-array design," *IEEE Trans. Antennas Propag.*, vol. 71, no. 2, pp. 1578–1589, Feb. 2023.

[41] Y. Liu et al., "An efficient method for antenna design based on a self-adaptive Bayesian neural network-assisted global optimization technique," *IEEE Trans.actionsAntennas Propag.*, vol. 70, no. 12, pp. 11375–11388, Dec. 2022.

[42] M. O. Akinsolu, B. Liu, V. Grout, P. I. Lazaridis, M. E. Mognaschi, and P. D. Barba, "A parallel surrogate model assisted evolutionary algorithm for electromagnetic design optimization," *IEEE Trans. Emerg. Topics Comput. Intell.*, vol. 3, no. 2, pp. 93–105, Apr. 2019.

[43] B. Liu, M. O. Akinsolu,N. Ali, and R. Abd-Alhameed, "Efficient global optimisation of microwave antennas based on a parallel surrogate model-assisted evolutionary algorithm," *IET Microw., Antennas Propag.*, vol. 13, no. 2, pp. 149–155, Feb. 2019.

[44] Q. Hua et al., "A novel compact quadruple-band indoor base station antenna for 2G/3G/4G/5G systems," *IEEE Access*, vol. 7, pp. 151350–151358, 2019.

[45] M. Alibakhshikenari et al., "Dual-polarized highly folded bowtie antenna with slotted self-grounded structure for sub-6 GHz 5G applications," *IEEE Trans. Antennas Propag.*, vol. 70, no. 4, pp. 3028–3033, Apr. 2022.

[46] J. Zhang,M. O. Akinsolu, B. Liu, and G. A. E. Vandenbosch, "Automatic AI-driven design of mutual coupling reducing topologies for frequency reconfigurable antenna arrays," *IEEE Trans. Antennas Propag.*, vol. 69, no. 3, pp. 1831–1836, Mar. 2021.

[47] J. Zhang, M. O. Akinsolu, B. Liu, and S. Zhang, "Design of zero clearance SIW endfire antenna array using machine learning-assisted optimization," *IEEE Trans. Antennas Propag.*, vol. 70, no. 5, pp. 3858–3863, May 2022.

[48] Q. Zheng, C. Guo, J. Ding, M. O. Akinsolu, B. Liu, and G. A. E. Vandenbosch, "A wideband low-RCS metasurface-inspired circularly polarized slot array based on AI-driven antenna design optimization algorithm," *IEEE Trans. Antennas Propag.*, vol. 70, no. 9, pp. 8584–8589, Sep. 2022.

[49] X. Li and K. M. Luk, "The grey wolf optimizer and its applications in electromagnetics," *IEEE Trans. Antennas Propag.*, vol. 68, no. 3, pp. 2186–2197, Mar. 2020.
[50] P. I. Lazaridis et al., "Comparison of evolutionary algorithms for LPDA antenna optimization," *Radio Sci.*, vol. 51, no. 8, pp. 1377–1384, Aug. 2016.
[51] A. A. Al-Azza, A. A. Al-Jodah, and F. J. Harackiewicz, "Spider monkey optimization: A novel technique for antenna optimization," *IEEE Antennas Wireless Propag. Lett.*, vol. 15, pp. 1016–1019, 2016.
[52] V. Grout, M. O. Akinsolu, B. Liu, P. I. Lazaridis, K. K. Mistry, and Z. D. Zaharis, "Software solutions for antenna design exploration: A comparison of packages, tools, techniques, and algorithms for various design challenges," *IEEE Antennas Propag. Mag.*, vol. 61, no. 3, pp. 48–59, Jun. 2019.
[53] B. Liu et al., "An efficient method for complex antenna design based on a self-adaptive surrogate model-assisted optimization technique," *IEEE Trans. Antennas Propag.*, vol. 69, no. 4, pp. 2302–2315, Apr. 2021.
[54] B. Liu, D. Zhao, P. Reynaert, and G. G. E. Gielen, "GASPAD: A general and efficient mm-Wave integrated circuit synthesis method based on surrogate model assisted evolutionary algorithm," *IEEE Trans. Comput.-Aided Design Integr. Circuits Syst.*, vol. 33, no. 2, pp. 169–182, Feb. 2014.
[55] "CST microwave StudioR 2021." 2021. [Online]. Available: https://www.3ds.com/products/simulia/cst-studio-suite
[56] W. Chen, Q. Wu, C. Yu, H. Wang, and W. Hong, "Multibranchmachine learning-assisted optimization and its application to antenna design," *IEEE Trans. Antennas Propag.*, vol. 70, no. 7, pp. 4985–4996, Jul. 2022.
[57] S. Koziel, N. Çalık, P. Mahouti, and M. A. Belen, "Low-cost and highly accurate behavioralmodeling of antenna structures by means of knowledge-based domain-constrained deep learning surrogates," *IEEE Trans. Antennas Propag.*, vol. 71, no. 1, pp. 105–118, Jan. 2023.
[58] S. Koziel and A. Pietrenko-Dabrowska, "Accelerated gradient-based optimization of antenna structures using multifidelity simulations and convergence-based model management scheme," *IEEE Trans. Antennas Propag.*, vol. 69, no. 12, pp. 8778–8789, Dec. 2021.
[59] A. Bekasiewicz and S. Koziel, "Reliable multistage optimization of antennas for multiple performance figures in highly dimensional parameter spaces," *IEEE Antennas Wireless Propag. Lett.*, vol. 18, pp. 1522–1526, 2019.
[60] A. Pietrenko-Dabrowska and S. Koziel, "Antenna modeling using variable-fidelity EM simulations and constrained co-kriging," *IEEE Access*, vol. 8, pp. 91048–91056, 2020.
[61] M. T. M. Emmerich, K. C. Giannakoglou, and B. Naujoks, "Single- and multiobjective evolutionary optimization assisted by Gaussian random field metamodels," *IEEE Trans. Evol. Comput.*, vol. 10, no. 4, pp. 421–439, Aug. 2006.
[62] J. E. Dennis and T. Virginia. "Managing approximation models in optimization," in *Multidisciplinary Design Optimization: State-of-the-Art*, vol. 5. Philadelphia, PA, USA: SIAM, 1997, pp. 330–347.
[63] R. Storn and K. Price, "Differential evolution—A simple and efficient heuristic for global optimization over continuous spaces," *J. Global Optim.*, vol. 11, no. 4, pp. 341–359, 1997.
[64] M. Stein, "Large sample properties of simulations using Latin hypercube sampling," *Technometrics*, vol. 29, no. 2, pp. 143–151, 1987.
[65] D. Agahi and W. Domino, "Efficiency measurements of portable-handset antennas using the wheeler cap," *Appl. Microw. Wireless*, vol. 12, pp. 34–43, Jun. 2000.
[66] "Ray optics simulation." Accessed: 7 Mar. 2023. [Online]. Available: https://phydemo.app/ray-optics/simulator/
[67] H. Vettikalladi, O. Lafond, and M. Himdi, "High-efficient and high-gain superstrate antenna for 60-GHz indoor communication," *IEEE Antennas Wireless Propag. Lett.*, vol. 8, pp. 1422–1425, 2009.
[68] R. Xu et al., "A review of broadband low-cost and high-gain low-terahertz antennas for wireless communications applications,"*IEEE Access*, vol. 8, pp. 57615–57629, 2020.
[69] Q. Guo and H. Wong, "A millimeter-wave Fabry–Pérotcavity antennausing fresnel zone plate integrated PRS," *IEEE Trans. Antennas Propag.*, vol. 68, no. 1, pp. 564–568, Jan. 2020.
[70] M. U. Afzal, K. P. Esselle, and B. A. Zeb, "Dielectric phase-correcting structures for electromagnetic band gap resonator antennas," *IEEE Trans. Antennas Propag.*, vol. 63, no. 8, pp. 3390–3399, Aug. 2015.

**KOUSHIK DUTTA** (Senior Member, IEEE) received the B.Sc. degree (Hons.) in physics and the B.Tech., M. Tech., and Ph.D. degrees in radio physics and electronics from the University of Calcutta in 1999, 2002, 2004, and 2017 respectively. He is currently an Associate Professor with the Department of Electronics and Communication Engineering, Netaji Subhash Engineering College, Kolkata, India. Prior to this, in 2021, he served as a Visiting Scientist with the Department of Electrical and Computer Engineering, University of Central Florida, USA. He has researched developing high-gain Fabry-Perot cavity antenna with a new concept and theory. He has published over 45 papers in top peer-reviewed journals and conferences. He has recently received the Core Research Grant (CRG) funded by SERB, DST, Government of India. His current research interests include dielectric resonator antennas, Fabry-Perot cavity antennas, lens antennas, phased array antennas, reconfigurable intelligent surface, and beam scanning antennas for millimeter wave 5G/6G applications. He has received the National Fellowship from MHRD, India, in 1999, the Outstanding Volunteer Award from IEEE AP-MTT Kolkata Chapter in 2017, and three best paper awards in IEEE conferences. He took the responsibilities of several IEEE organizational units under IEEE Kolkata Section. He is presently associated with the editorial boards of several International Journals and an Associate Editor of the *IETE Journal of Research* and *International Journal of Electrical and Computer Engineering*. He served as the Chair of IEEE AP-MTT Joint Chapter of Kolkata from 2022 to 2023 and the Student Activity Chair of IEEE Kolkata Section from 2017 to 2022. He served as the Organizing Chair of IEEE International Conferences ICCE 2020, and AESPC 2021 and 2023. He is a Life Member of the Institute of Engineers, India, and the Indian Radio Science Society.

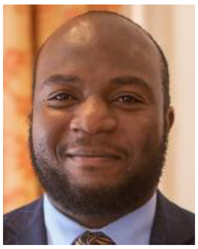

**MOBAYODE O. AKINSOLU** (Senior Member, IEEE) received the M.Sc. degree (with Distinction) in electrical and electronic engineering from the University of Bradford, U.K., in 2014, following his undergraduate studies and mandatory national service in Nigeria, the Ph.D. degree with commendation through the partnership between Wrexham University, U.K. and the University of Chester, U.K., working on a studentship project involving the University of Birmingham, U.K., and the University of Bradford in 2019, and the Postgraduate Certificate (with Distinction) in learning and teaching in higher education from Wrexham University in 2021. He is a Senior Lecturer (Associate Professor) of Electronic and Communication Engineering with Wrexham University. He is also a Visiting Scholar with Lead City University, Nigeria, and an External Examiner with Regional Maritime University, Ghana. Before joining Wrexham University, he worked as a Research Fellow (Industrial Attaché) and a Visiting Researcher with the Centre for Satellite Technology Development, National Space Research and Development Agency, Nigeria, and the RFID Research Centre, African University of Science and Technology, Nigeria, respectively. From 2022 to 2023, he led a Data Study Group with The Alan Turing Institute, U.K. His research interests include applied artificial intelligence, antennas, machine learning-assisted optimization, simulation-driven design, and engineering management. He has published several articles, all focusing on topics aligned with his research pursuits. He has served as a short course instructor on the artificial intelligence-driven design of antennas at prestigious technical events, such as the IEEE AP-S/URSI, EuMW, and EuCAP. He is a Chartered Engineer in membership of the IET (Engineering Council, U.K.), a Fellow of the HEA (AdvanceHE, U.K.), and a registered Engineer with the COREN.

**PUNEET KUMAR MISHRA** (Senior Member, IEEE) received the M.Tech. degree in RF and microwave from the Indian Institute of Technology Roorkee, India, in 2004. Since 2004 he has been with U R Rao Satellite Centre, Bengaluru, India, and heading its Satellite Antenna Characterization, Test and Design Section. He has rich experience in RF characterization of 50 Satellites, 350+ antennas, and radomes. He has indigenously developed C-Band, Ku-Band, and Ka-Band Compact range feeds to meet various requirements of ISRO's satellite program. He has played a pivotal role in establishing a satellite-level EMC facility and Asia's largest Magnetic Field Measurement Facility. He conceived and conceptualized the World's first compact range with 10 m quiet zone going to be commissioned in 2025. He has received the IETE-IRSI Young Scientist Award in 2012, the ISRO Young Scientist Award in 2013, the ASI-ISRO Space Gold Medal in 2014, the GE Foundation Award for Academic Excellence and Leadership from 2002 to 2004, the IEEE MGA Achievement Award in 2017, and six best paper awards. He has indigenously developed a payload to study the RF blackout phenomenon during the re-entry of space vehicles. He has also successfully developed Indigenous BusBars for high-power satellites, which are successfully used in multiple spacecraft. He is a passionate Volunteer and served the IEEE Bangalore Section in various capacities including Chair 2020 and IEEE India Council as the Vice Chair and a Secretary. He is currently serving as the BoG of Global IEEE AESS, the Vice Chair (Technical Activities), an India Council, the Chair, the IEEE AESS Bangalore Joint Chapter, and a member of Global Committees of IEEE Industry Engagement. He is a Fellow of IETE and IE(I) and a Life Member of ASI.

**BO LIU** (Senior Member, IEEE) received the B.Eng. degree from Tsinghua University, Beijing, China, in 2008, and the Ph.D. degree from the University of Leuven, Leuven, Belgium, in 2012. From 2012 to 2013, he was a Humboldt Research Fellow with the Technical University of Dortmund, Dortmund, Germany. In 2013, he was an Assistant Professor with Wrexham Glyndwr University, Wrexham, U.K., where he was promoted to a Reader in 2016. He is currently a Professor of Electronic Design Automation with the University of Glasgow, Glasgow, U.K. He is also a Senior Honorary Fellow with the University of Birmingham, Birmingham, U.K. He has authored or coauthored one book and more than 90 papers in renowned international journals, edited books, and conference proceedings. His research interests include artificial intelligence (AI)-driven design methodologies of analog/RF integrated circuits, microwave devices, evolutionary computation, and machine learning. In terms of AI-driven antenna design, he is a main inventor and a designer of the surrogate model assisted differential evolution for antenna synthesis (SADEA) algorithm series.

**DEBATOSH GUHA** (Fellow, IEEE) received the B.Tech. and M.Tech. degrees in radio physics and electronics, and the Ph.D. degree in microwave engineering from the University of Calcutta in 1987, 1989, and 1994, respectively. He started his career in Telecommunication Industry in India. He is currently a Professor of Radio Physics and Electronics with the University of Calcutta, where he is the Dean of the Faculty of Engineering and Technology. He is also an Adjunct Professor with the National Institute of Technology Jaipur, India. He joined the University of Calcutta as an Assistant Professor in 1994. Later on, he spent about a couple of years with the Royal Military College of Canada, Kingston, ON, Canada, as a Visiting Research Professor. He has researched in developing microstrip and dielectric resonator antenna technologies. Defected ground structure-inspired antenna is one of his major areas of contribution. More than 200 technical papers in IEEE journals and conferences along with a couple of books on planar antenna techniques published by IEEE Press/Wiley are to his credit. Several of his invented techniques are now commonly used by industries and the leading research and development Labs. A novel high gain wireless antenna developed by him has been a commercial product since 2007 in the North American market. He has mentored more than 25 doctoral and postdoctoral students over the last two decades. His current research interests include defected ground structure and metasurface induced antenna, hybrid subarray structures, artificial intelligence and machine learning based antenna designs, and advanced resonance cavity antenna techniques. He is a recipient of some notable awards which include the IETE Ram Lal Wadhwa Award in 2016, the Raj Mittra Travel Grant Award in 2012, the URSI Young Scientist Award in 1996, and the Jawaharlal Nehru Memorial Fund Prize in 1984. He served as an Associate Editor for IEEE TRANSACTIONS ON ANTENNAS AND PROPAGATION and IEEE ANTENNAS AND WIRELESS PROPAGATION LETTERS and as a Section Editor for *IEEE Antennas and Propagation Magazine*. He served as a member of IEEE AP-S Fields Award Committee from 2017 to 2019 and as the Co-Chair of AP-S Technical Committee on Antenna Measurements from 2021 to 2023. He has been serving as the Indian National Chair for URSI Commission B since 2014. He served the IEEE Kolkata Section as the Chair from 2013 to 2014, and the Founding Chair of AP/MTT-S Kolkata Chapter in 2004. He is a Co-Founder of IEEE Microwaves Antennas and Propagation Conference MAPCon in India in 2022. Prior to MAPCon, he conceptualized and established IEEE Applied Electromagnetics Conference in 2007 as a major biennial IEEE meeting in India and IEEE Indian Antenna Week as a yearly international workshop in 2010. He is a Distinguished Lecturer of the IEEE Antennas and Propagation Society. He is an Abdul Kalam Technology Innovation National Fellow, Government of India and is also a Fellow of all four Indian National Academies for Science and Engineering which include the Indian National Science Academy; the Indian Academy of Sciences, Bengaluru; The National Academy of Sciences, Allahabad; and the Indian National Academy of Engineering. He has been currently serving the IEEE AP-S AdCom as the Chair of AP-S Member and Geographic Activities Committee.